Cement & Concrete Composites 44 (2013) 77–92

Contents lists available at SciVerse ScienceDirect

Cement & Concrete Composites

journal homepage: www.elsevier.com/locate/cemconcomp

Characterization of morphology and texture of several amorphous nano-silica particles used in concrete

G. Quercia [a,b,*], A. Lazaro [b], J.W. Geus [c], H.J.H. Brouwers [b]

[a] Materials innovation institute (M2i), Mekelweg 2, P.O. Box 5008, 2600 GA Delft, The Netherlands
[b] Eindhoven University of Technology, Department of the Built Environment, P.O. Box 513, 5600 MB Eindhoven, The Netherlands
[c] University of Utrecht, Debye Institute for Nanomaterials Science, 3584 CH Utrecht, The Netherlands

ARTICLE INFO

Article history:
Received 30 August 2012
Received in revised form 14 May 2013
Accepted 16 May 2013
Available online 31 May 2013

Keywords:
Nano-silica
Texture
Particle size
Surface area
Slump-flow
Workability

ABSTRACT

In the present research, the morphological and the textural characteristics of different amorphous nano-silica's used in concrete were studied. To conduct a detailed characterization of the main properties of micro- and nano-silica, seven selected silica samples produced by different methods were studied thoroughly. The resulting characteristics, such as shape, particle size, specific surface area, density, and pore-size (distribution), are related and compared. Finally, the effects of the nano-silica characteristics on the slump-flow diameter and mechanical properties of standard mortars are discussed. It was found that the main parameters that influence the slump-flow diameter and the final mechanical properties of cement mortars are the specific surface area, the micropore volume and the average size of the primary particles of the silica's. In addition, no direct influence on the mortar properties related with the silica's pore diameter and pore-size (distribution) was found.

© 2013 Elsevier Ltd. All rights reserved.

1. Introduction

The properties of freshly prepared concrete, such as flow behavior and workability, are governed by the particle size distribution of the solid constituents. Moreover, the properties of the concrete in the hardened state, such as strength and durability, are affected by the grading of the mix and the resulting particle packing [1]. One way to further improve the packing is to increase the solid size range. Possible materials which are currently available to raise the size range are limestone and silica fines, like micro-silica (mS) and nano-silica (nS). The main characteristics of silica fines, such as the particle size distribution, specific density, specific surface area, pore structure, and reactivity (surface silanol groups), depend on the production method [2].

For the design of a concrete mix, it is important to consider the fine particles, as they have an influence on the water demand and, consequently, on the fresh and hardened concrete properties. In the granular state, part of the total water content is present as an adsorbed layer that surrounds the fine particles, while the balance of the water is required to fill the remaining void fraction (Ψ). Since the fine powders are the particles with the largest specific surface area, the fine particles most strongly affect the total water demand of a concrete mix. The total water content influences the properties of the final concrete, such as porosity, permeability, and compressive strength. To achieve an optimum result, the powders should have a low water demand. In recent years, the application of nanotechnology in building materials has increased exponentially [3]. One of the most used and common nano-material is amorphous silica with particle sizes in the nano-range (nS). It has been reported [2,4] that addition of nano-silica (nS) increases the compressive strength and reduces the permeability of hardened concrete. The effects are caused by the pozzolanic properties of nS particles, which results in finer hydrated phases (C—S—H gel), and a densified microstructure owing to nano-filler and anti-leaching effects.

Different types of micro- and nano-silica additives are available on the market for use as admixtures in high performance (HPC) and self compacting concrete (SCC). The silica additives are produced by different procedures or routes. One production method is based on a so-called sol–gel process (organic or water route) at room temperature [3]. In this process, the starting materials (mainly Na_2SiO_3 or organosilicon compounds, like TMOS/TEOS) are brought in as a solvent, and subsequently the pH of the solution is increased (or decreased) to the gelling point of silica. The produced gel is aged and collected by filtration. The gel is dried to a xerogel and calcined or re-dispersed in water with a stabilizing agent (Na, K, NH_3, etc.) to produce a concentrated dispersion (20–50% solid content) suitable for use in the concrete industry [3,5].

An alternative production method is based on the volatilization of silica between 1500 and 2000 °C by reducing quartz (SiO_2) in an

* Corresponding author at: Materials innovation institute (M2i), Mekelweg 2, P.O. Box 5008, 2600 GA Delft, The Netherlands. Tel.: +31 402472323.
E-mail address: g.quercia@tue.nl (G. Quercia).

0958-9465/$ - see front matter © 2013 Elsevier Ltd. All rights reserved.
http://dx.doi.org/10.1016/j.cemconcomp.2013.05.006

electric arc furnace. Another procedure performed on a large scale involves passing $SiCl_4$ in a hydrogen–oxygen flame (flame hydrolysis process), where the reaction between the resulting water vapor and $SiCl_4$ proceeds forming pyrogenic silica particles [6]. Furthermore, nS is produced as a byproduct during the manufacturing of silicon and ferro-silicon alloys, where the silica vapor is condensed and collected in a cyclone [7,8]. Nano-silica produced by this method (commonly referred as silica fume) is a very fine powder consisting of spherical particles or microspheres with a main diameter of 150 nm and thus a high specific surface area (15–25 m^2/g). Finally, nS can also be produced by a precipitation procedure. According to this method, nS is precipitated by acidifying a precursor solution at temperatures between 50 and 100 °C (precipitated silica). This method, which was first developed by Iler [9], uses different precursors, such as sodium silicates (Na_2SiO_3), burned rice husk ash (RHA) and semi-burned rice straw ash (SBRSA), magnesium silicates, and others [8,9].

In addition, nano-silica (nS) can be synthesized via an alternative production route first established by Schuiling [10] and later elaborated by Lieftink [11] and Jonckbloedt [7]. Recently, Lazaro et al. [12] improved the feasibility of this process. In the synthesis route, basically, olivine and sulfuric acid are mixed, whereby precipitated silica is synthesized containing primary particles between 6 and 30 nm strongly agglomerated.

Even though there are several studies that describe the main properties of nano-silica particles [11,13–15], most publications focus on applications of nano-silica in catalysis and not on its use in concrete. The knowledge of the main physicochemical characteristics of silica additives, such as morphology and texture, are important parameters for the design, and for the prediction of the water demand of concrete mixes.

The objective of the present investigation is to describe and to determine the physicochemical properties of different micro- and nano-silica additives, and to contribute to the understanding of the influence of the main characteristics on the properties of concrete. In the field of construction and building materials, a detailed and profound consideration of micro- and nano-silica, to the author's knowledge, has never been reported. To generate a detailed characterization of the main properties of micro- and nano-silica, seven selected silica samples produced by different routes were thoroughly studied.

The techniques to establish the morphological characteristics of the silicas include: scanning electron microscopy (SEM), scanning and transmission electron microscopy (STEM and TEM, respectively), elemental analysis by energy-dispersive X ray spectrometry (EDS), helium and glass pycnometry for density determination, particle size distribution (PSD) by laser light scattering (LLS), and dynamic light scattering (DLS). For the textural characteristics, the physical adsorption of nitrogen was measured to determine the specific surface area calculated according to the Brunauer–Emmett–Teller (BET) procedure [16]. The external surface area was computed by the *t*-plot method based on [17], and the pore-size and distribution by the Barrett–Joyner–Halenda (BJH) method [18]. Finally, standard mortars were prepared and tested for their fresh (slump-flow) and hardened behavior (28-day flexural and compressive strength). The resulting characteristics were related and compared for the selected micro- and nano-silica samples.

2. Materials and experimental methods

2.1. Materials

Six different silicas (amorphous SiO_2 particles) were selected to determine their physicochemical characteristics. The samples studied were chosen to cover a wide range of particles sizes and production routes, mainly classified as nano-silica when their particles sizes were between 1 and 700 nm and as micro-silica when the samples contain a high fraction of particle sizes in the micro-range or exhibit a specific surface area lower than 35 m^2/g, maximum limit according to [19].

The samples were grouped and named as follows: two colloidal nano-silica suspensions prepared by the waterglass route (samples CnS-1 and CnS-2); one fumed nano-silica in powder form (PnS-3), one standard micro-silica in slurry form (PmS-4); and two pyrogenic silica samples, nano-silica (PmS-5) and micro-silica (PmS-6), with different BET specific surface area (SSA_{BET}), also in powder form. In addition, one sample prepared by dissolution of olivine mineral in acid (POnS-7) was studied for comparison. Tables 1 and 2 represent their general characteristics (taken from the product data sheets) and their chemical composition (determined by XRF), respectively.

2.2. Experimental methods

2.2.1. Particle morphological characteristics

Size and morphology of the silica fines were analyzed using a scanning electron microscope (FEI XL-30 FEG-SEM) and a transmission electron microscope (Tecnai model 20FEG), both equipped with a Schottky field emission gun operated at 20 and 200 keV, respectively. Furthermore, a elementary analysis was performed using an EDAX® energy-dispersive spectroscopy (EDS) device.

2.2.2. Particle-size distribution (PSD) and specific surface area (SSA) of silica

a. Particle-size distribution (PSD). Measurement of particle-size distributions is a major challenge for the powder technologist. There are numerous methods suitable for its determination, but laser light scattering (LLS) and dynamic light scattering (DLS) are commonly employed for fine powders. Laser light diffraction was used to determine the particle size distribution of the micro- and nano-silica samples. This technique has become the dominating method for the characterization of powders in both research and industry [20]. In this study the particle size distribution of the silica samples, PnS-3, PmS-4, PmS-5 and PmS-6 was measured in aqueous dispersion with a Malvern™ Mastersizer™ 2000 laser light diffraction device, using the Mie scattering theory for the calculation of the particle size distribution and following the ISO standard 13320-1 [21]. A Hydro S unit was used to disperse the samples. A spherical shape was assumed to calculate the particle size distribution and to compute the specific surface area (SSA_{Sph}) for all the tested silica samples based on the arithmetic mean diameter of each size class and following the procedure described by [22].

Dynamic light scattering (DLS), sometimes referred to as photon correlation spectroscopy (PCS) or quasi-elastic light scattering (QELS), is a non-invasive, well-established technique for measuring the size of molecules and particles typically in the submicron region. The diameter which is measured by DLS is termed the hydrodynamic diameter ($D_{(H)}$) and reflects the rate of diffusion of a particle within a fluid. The diameter obtained by this technique is the size of a sphere that has the same translational diffusion coefficient as the particle being measured. The translational diffusion coefficient depends not only on the size of the particle "core", but also on the layer of tightly bound water molecules, the surface structure as well as the concentration, and the type of ions in the medium. Consequently, the particle size is likely to be larger than measured by electron microscopy [23]. The particle-size distribution of the two colloidal nano-silicas (CnS-1 and CnS-2), and the olivine nano-silica (POnS-7) were measured in liquid dispersion (water) using a dynamic light scattering device Malvern™ Zetasizer™ Nano ZS according to [23]. A conventional cell was used for particle size measurement (distribution in volume).

Table 1
Specification and general characteristics of the tested amorphous silica's.

Name	CnS-1	CnS-2	PnS-3	PmS-4	PmS-5	PmS-6	POnS-7
Type	Colloidal	Colloidal	Powder	Powder$^{(£)}$	Powder	Powder	Powder
Production route	Water glass	Water glass	Pyrolysis	Fume	Pyrolysis	Pyrolysis	Olivine dissolution
Specific density (g/cm^3)$^{(*)}$	–	–	2.2	2.3	2.2–2.3	2.2–2.3	1.9–2.1
Bulk density (g/cm^3)	1.05$^{(*)}$	1.40$^{(*)}$	0.09–0.11$^{(*)}$	1.40$^{(*)}$	09–0.11$^{(*)}$	0.15–0.70$^{(*)}$	0.10
pH	9–11	9–11	5$^{(+)}$	5–7	5$^{(+)}$	5–7$^{(+)}$	3–6$^{(+)}$
Solid content (% w/w)	15$^{(*)}$	48–52$^{(*)}$	–	48–50$^{(*)}$	–	–	–
Viscosity (mPa s)	<50$^{(*)}$	<50$^{(*)}$	–	–	–	–	–
Loss on ignition (L.O.I.)	6.4	3.8	0.5$^{(*)}$	4$^{(*)}$	0.5$^{(*)}$	0.5$^{(*)}$	9.0
BET (m^2/g)	200–500	50	50	15–35	50	10	100–400
Particle sizes (μm)	–	–	<0.4	–	–	–	<0.1

(–): Not displayed by product data sheet or not applicable; (+): 4% m/m in water; (*): values taken from product data sheet; (£): applied in slurry form with 50% solid according to EN 13263-1, 2009 [19].

Table 2
Chemical composition by X-ray fluorescence (XRF) of the studied amorphous silica's.

Name	CnS-1	CnS-2	PnS-3	PmS-4	PmS-5	PmS-6	POnS-7
SiO_2	97.29	99.33	99.55	96.12	99.62	99.55	98.97
Al_2O_3	0.15	0.07	<0.01	0.86	0.18	0.30	0.05
Fe_2O_3	0.03	0.03	0.34	0.34	0.05	0.03	0.28
MnO	–	–	–	0.04	–	–	–
MgO	<0.01	<0.01	<0.01	0.53	<0.01	<0.01	0.31
CaO	0.02	0.01	<0.01	0.39	0.01	0.01	0.04
Na_2O	2.15	0.35	<0.01	0.21	<0.01	0.01	<0.01
K_2O	0.27	0.09	<0.01	1.05	0.04	0.01	0.04
TiO_2	0.02	0.02	0.01	<0.01	0.01	<0.01	0.01
P_2O_5	0.01	0.01	0.01	0.07	0.02	0.01	0.02
Cr_2O_3	0.01	0.01	0.01	<0.01	0.01	0.02	0.03
SO_3	0.03	0.05	0.03	0.36	0.03	0.03	0.24
C-Total	0.08	0.08	0.08	0.66	0.08	0.07	0.03

b. Computed specific surface area (SSA_{Sph}). The specific surface area (*SSA*) is a property of solids which is the total surface area of a material per unit of mass (m^2/g), solid or bulk volume (m^2/m^3), or cross-sectional area. Taking into account the specific density ρ^{spe} (Table 1), the computed spherical specific surface area SSA_{Sph} can also be expressed as area per unit volume (cm^2/cm^3). Beside the mass and solid volume, the SSA_{Sph} can also be related to the bulk volume (taking into account the void fraction). The SSA_{Sph} was derived indirectly from the particle size distribution using the procedure described by McCabe and Smith [24] and later by Hunger [22]. This procedure takes into account the specific density of the silica and cement, and the measured particle size distribution to compute the SSA_{Sph} of all materials using the following equation:

$$SSA_{Sph} = 6\sum_{i=1}^{n}\frac{w_i}{D_{i,arith}\cdot\rho^{spe}} \quad (1)$$

where w_i is the corresponding mass of the grain fraction i and $D_{i,arith}$ is the arithmetic mean diameter between two consecutives sieve size fractions, D_i and D_{i+1}. The results are shown in Table 3.

c. Specific surface areas by N_2 physisorption analysis (SSA_{BET}, $SSA_{t\text{-plot}}$ and SSA_{ext}). Gas sorption (both adsorption and desorption) is the most common method for determining the surface area of powders as well as the pore-size distribution of porous materials. A Micromeretics Tristar 3000 equipment, using N_2 and an evacuation period of time of 12 h at 120 °C, was used for the gas physisorption analysis. Using the BET theory [16] and the standard procedure described in [25], the specific surface area (SSA_{BET}) of the silica samples was determined.

The nitrogen sorption data was used to compute the total specific surface area ($SSA_{t\text{-plot}}$), the external specific surface area (SSA_{ext}) and the micropores volume (V_{MP}) following the *t*-plot method described by [26]. The statistical thickness (t_{layer}) of the adsorbed gas layer at a given value of $x = P/P_0$, calculated using the model proposed by [27], was plotted against the volumes of liquid taken up (n_v). The external specific surface area (SSA_{ext}) in m^2/g, defined here as the surface area of pores larger than micropores, was determined from the slope of the first straight line segment within the pressure region ($0.10 < P/P_0 < 0.35$) using the following equation:

$$n_v(x) = V_{MP} + k_1\cdot SSA_{ext}\cdot t_{layer}(x) \quad (2)$$

where V_{MP} is the adsorption in saturated micropores (micropore volume), and k_1 is a constant that depends on the units and is equal to the inverse value of 1.5468 (cm^3/m^2 nm).

The total specific surface area ($SSA_{t\text{-plot}}$) that includes all the pores was determined from the slope of the straight line segment passing though the origin at the pressure regions (P/P_0) lowers than 0.10 using the following equation:

$$n_v(x) = k_1\cdot SSA_{t\text{-plot}}\cdot t_{layer}(x) \quad (3)$$

where k_1 is the same constant previously defined.

Finally, using the different specific surface areas, the size of the primary and agglomerated particles were calculated based on [28] as follows:

$$d_i = \frac{6000}{\rho\cdot SSA_i} \quad (4)$$

where d_i is the particle or agglomerate diameter size (nm), ρ the density and SSA_i is the specific surface area determined by the BET method (SSA_{BET}) or by geometrical considerations (SSA_{Sph}).

Table 3
Properties of the studied amorphous silica's.

Name	Particle size range by SEM/(S)TEM (nm)	Particle size range by LLD and DLS (nm)	SSA_{Sph} (cm^2/cm^3) × 10^{-4}	Agglomerates particle size (d_{agg}) (nm)
CnS-1	2–50	0.9–2.3	364	1.6
CnS-2	19–156	79–186	46	124
PnS-3	14–187	73–291	48	215
PmS-4	14–332	78–13000	34	169
PmS-5	23–391	194–446	22	265
PmS-6	29–658	348–12,000	8	795
POnS-7	10–720	34–356	48	104

2.2.3. Pore-size and distribution (BJH method)

Data obtained from the nitrogen physical adsorption isotherms was used to determine the pore-size distribution and the surface area of the pore of a specific radius (r_p) of the silica samples. For this, the Kelvin equation, which describes the pore radius considering the pore as a cylinder, was used [18]:

$$\log\left(\frac{P}{P_0}\right) = \frac{-2\sigma V_N}{RT}\cdot\frac{1}{r_p} \quad (5)$$

where σ is the surface tension, V_N the molar volume of liquid nitrogen, R the gas constant and T is the absolute temperature in K. Furthermore, taking into account the thickness (t_{layer}) in nm of the liquid nitrogen condensate in a relative pressure interval in the wall of the pores, gives as described by Halsey in [29]:

$$t_{layer} = 3.54\left[\frac{-5.00}{\ln(\frac{P}{P_0})}\right]^{0.333} \quad (6)$$

The pore diameter in nanometer (d_p) is defined for each interval of relative pressure as:

$$d_p = 2(r_p + t_{layer}) \quad (7)$$

Inserting Eq. (6) in (7) and using the BJH method described by [18], the pore diameter for each relative pressure interval where condensation of liquid nitrogen occurred were derived.

The BJH method was applied for the adsorption and desorption isotherms to derivate the pore-size and distribution only as comparison purpose. It is known that this method take into account several assumptions [30,31]. Nevertheless, it is still the most widely used method to characterize the pores in the range 2–50 nm.

2.2.4. Specific density by glass and helium pycnometry

The densities of all the samples were measured according to the norm DIN EN 1097-7 [32] using a calibrated glass pycnometer. For comparison purpose, a helium pycnometer AccuPyc® II 1340 from Micromeretics was used to determine the specific density of the powder silica samples. Gas pycnometry is a commonly used analytical technique that is based on the displacement of gas to measure the sample's volume accurately. Before the density measurements, the samples were dried and degassed at 105 °C for 24 h. Helium was used as the displacement medium. Ten purges of the system were performed to ensure the equilibrium and to complete a total degassing of the sample. This was followed by 12 consecutive volume measurements, which were then used to obtain the values of the average density.

2.2.5. Behavior of standard mortars with nano-silica in fresh and hardened states

To determine the effects of different types of nano-silica on the behavior of mortars in fresh and hardened states, different standard cement mortars were prepared and tested following the procedure established in [33]. A 7% replacement based on the weight of cement (bwoc) was selected based on the procedure described by [34]. Three standard prisms for each nano-silica type were tested following the mix designs presented in Table 6. The superplasticizer (SP) content of the mixes was fixed at 0.6% based on the weight of binder (bwob) to determine the effect of the nano-silica on the slump-flow diameter of the pastes after 15 strokes of the flow-table. The flexural and compressive strengths of the prisms were determined after aging of 28 days under water. Finally, the relative pozzolanic index for each tested silica sample was computed based on the results of the standard cement mortar tests.

3. Results and discussion

3.1. Morphology, particle size distribution (PSD) and specific surface area (SSA_{Sph})

Fig. 1 represents the particle size and the morphology of all silica samples. For all nano- and micro-silica samples studied, a spherical shape is observed to be the main morphology. The morphology changes to slightly more angular particles when the particle size becomes smaller than 20 nm. The samples CnS-1 (Fig. 1a) and POnS-7 (Fig. 1g) exhibit a more irregular form and highly agglomerated state. The resultant SSA_{Sph}, average agglomerate size (d_{agg}) and the corresponding PSD of the silica samples are shown in Table 3 and are represented in Figs. 3–5.

The results presented in Table 3 and Fig. 2 illustrate that the selected silica samples have a diverse PSDs, varying between 1 nm and 13 μm. In general, the particle size range, as determined by the TEM measurements, is different to the DLS and LLS results. The difference is due to difficulties to completely break all particles clusters (agglomerates) during their dispersion in the aqueous media. Due to the fact that the interparticle forces increase with decrease drop in the particle size, the agglomerated state is larger with smaller elementary particles. Nevertheless, the production route also influences the aggregated state, as with the samples PmS-4, PmS-5 and PmS-6, which are produced at high temperatures. Consequently, the small particles are irreversibly clustered (sintered or welded), as was demonstrated by Diamond and Sahu [35] for similar type of silicas. This is evident in the particle size ranges determined by LLS (Table 3). On the other hand, PSDs are in line with the specific surface area computed considering geometrical considerations (SSA_{Sph}) and with the estimated average agglomerates size (Table 3). However, there is still a need to improve the dispersibility of nano-silica in water suspensions to obtain a better approximation between the particle-size ranges measured by DLS/LLS and by SEM/TEM/PSD. The problem with the dispersion is clearly apparent from Figs. 3 and 4, where the samples PmS-5 and POnS-7 exhibit a bimodal particle size distribution (strongly agglomerated state). Even though the primary particle size of the olivine nano-silica sample is about 11 nm (measured by TEM and later confirmed by BET measurements), the particle sizes measured by DLS/LLS are between 34 and 356 nm. The clustering of the elementary particles of silica POnS-7 leads to large differences between the aggregate sizes estimated from SSA_{Sph} (Table 3) and the observed and estimated primary particle size by TEM and SSA_{BET}, respectively (Table 4). The reason of the discrepancy is that the DLS method considers agglomerates or secondary particles as one particle, which leads to a lower SSA_{Sph}, whereas the BET method considers the total surface area including the micropores, which results in higher values for the surface area. The agglomerated state of olivine nano-silica has been previously reported [12,36–38]. This nano-silica is produced by dissolution of olivine in acid, where the pH is below the isoelectric point (point of zero charge). Under these conditions a colloidal solution is unstable and the silica particles agglomerate in 3D networks [9]. During this process, the elementary silica particles form chains due to formation of siloxane bridges (≡Si—O—Si≡) between the particles. The size of the agglomerates depends mainly on the pH of the solution during their precipitation, the particle-size distribution of the nano-silica, the mechanical or grinding treatment and the period of time that the silica has to agglomerate [9,12,39].

It is noteworthy to mention that some larger particles of about 20–200 nm were observed in electron micrographs of sample CnS-1. Even though these particles are present in the colloidal suspension, their concentration is less than 2%. For this reason, the DLS results show only particles from 0.9 to 2.3 nm when a volume concentration was considered in the computation of the PSD (Fig. 3). The DLS results are in line with Fig. 1a, in which only extremely small particles are exhibited.

The STEM images represented in Fig. 5c show formation of necks between the elementary silica particles, which is due to the high temperature during the collection of silica fume in dust cyclones. In addition, coalesce or aggregation of silica particles was also evident in the CnS-2 sample. Such aggregation is one of the main mechanisms reported for nano-silica synthesized by the waterglass route [9], which results in a lower specific surface area.

Electron diffraction to complement the analysis in the electron microscope revealed that all silica particles are amorphous, with one exception: the sample PmS-4, which is standard micro-silica

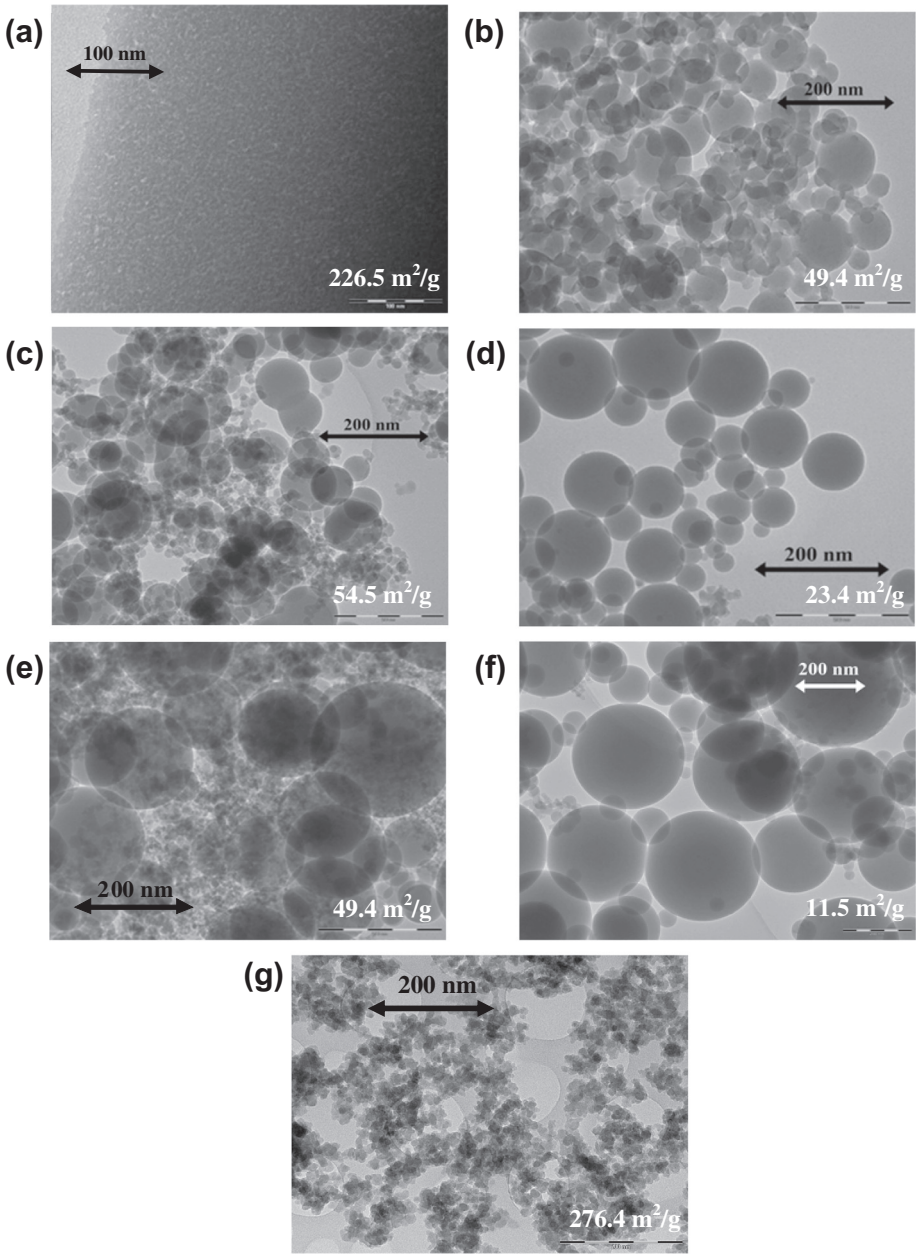

Fig. 1. Transmission electron micrographs of the studied silica samples, (a) CnS-1, (b) CnS-2, (c) PnS-3, (d) PmS-4, (e) PmS-5, (f) PmS-6 and (g) POnS-7.

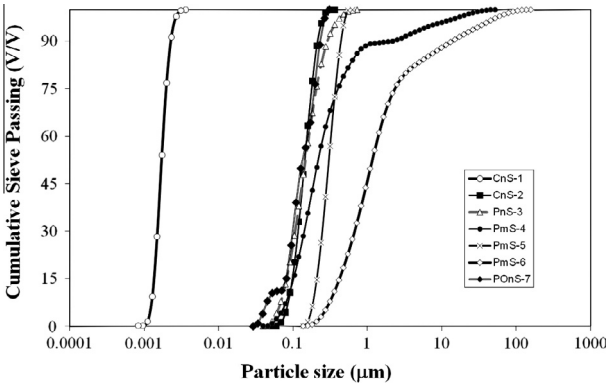

Fig. 2. Cumulative particle size distribution of the collected amorphous silica samples.

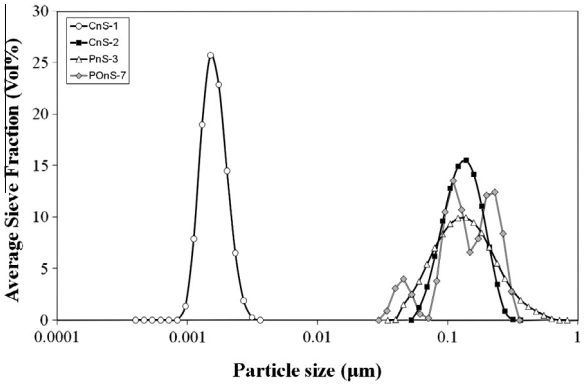

Fig. 3. Average sieve fraction by volume of the collected nano-silica samples.

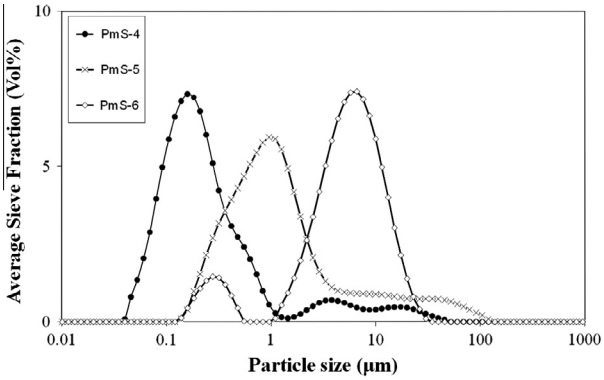

Fig. 4. Average sieve fraction by volume of the collected micro-silica samples.

Table 4
Computed textural parameters of the selected silica's.

Name	SSA_{BET} (m^2/g)	SSA_{ext} (m^2/g)	$SSA_{t\text{-plot}}$ (m^2/g)	V_{MP} (cm^3/g)	Primary particle size (d_{BET}) (nm)	Agglomeration ratio (d_{agg}/d_{BET})
CnS-1	232.8	216.5	226.5	0.0051	12.3	0.1
CnS-2	49.9	43.0	49.4	0.0026	54.7	2.3
PnS-3	56.2	49.2	54.5	0.0025	49.7	4.3
PmS-4	23.3	19.6	23.4	0.0014	114.3	1.5
PmS-5	50.2	42.9	49.4	0.0028	55.7	4.8
PmS-6	11.8	10.4	11.5	0.0005	226.9	3.5
POnS-7	262.6	193.6	276.4	0.0297	11.0	9.5

in slurry form. This standard silica displayed a small amount of a remnant crystalline species, which were detected by electron diffraction (pattern performed in the STEM). The remnant species are mainly composed of a crystalline SiO_2 (α-quartz) and some minor contaminants (rich in Fe, Ca and P), detected by the EDS analysis shown in Fig. 5d and confirmed later by XRF (see Table 2). These contaminants are normally found in standard micro-silica, as was reported by Friede [40] and Plank et al. [41].

The EDS analysis was performed to identify the main elements present in the bulk and surface of the silica (Figs. 5 and 6), which are in most cases silicon and oxygen. In a standard micro-silica (PmS-4) iron, calcium and phosphorus were identified as impurities (Fig. 5d). In this case, these elements possibly originate from the stabilization additive used for the silica slurries, which are mainly composed of phosphate compounds. For the POnS-7 sample, using the EDS technique, only magnesium was detected as an impurity. Nevertheless, other elements such as iron, aluminum and sulfur were identified based on the XRF results, as shown in Table 2. The presence of small amounts of these elements is expected, because this nano-silica is produced from the dissolution of olivine in sulfuric acid. The source of olivine is mainly a ground Dunite rock composed of $(Mg, Fe)_2SiO_4$ (90% by mass) and other inert minerals such as muscovite, enstatite, and serpentine (antigorite) [11].

The observed agglomerated state, which is different depending of the type and size of the primary silica particles, should affect mortar and concrete performance. For example, Diamond and Sahu [35] found that the agglomerates from micro-silica can be broken down into separated linked clusters of spheres, similar to the cluster identified in the present research, by sufficiently severe ultrasonic treatment. However, sintered spheres–spheres contacts are permanent. They also reported that the agglomerates can survive the ordinary concrete mixing, which it is not efficient in breaking down the agglomerates. As a consequence, the retained agglomerates in concretes clearly cannot participate in the filler effect attributed to micro-silica, and under some circumstances can act as damaging agent promoting alkali silica reaction (ASR) if reactive aggregates are used in the concrete recipe. This is the reason, that usually it is recommended to apply the micro- or nano-silica additives in slurry form together with a special mixing sequence as was concluded in the work of [42]. The objective is to avoid the presence of big agglomerates that can decrease the concrete performance. Table 4 presents the calculated agglomeration ratio (d_{agg}/d_{BET}), which can give indications about the degree of agglomeration of the different silica samples studied. Based on this value, we can conclude that the elementary silica particles in the samples PnS-3, PmS-5, PmS-6 and POnS-7 are highly agglomerated (ratio higher than 2), which can lead to undesired effects on the concrete performance if an appropriated mixing method is not applied. On the other hand, samples CnS-1, CnS-2 and PmS-4, display less agglomeration (lower than 2), which in theory should lead to a better dispersion of the particles during the concrete mixing. In the following sections, more details and discussions about the implications of the silica properties on the performance of concrete will be presented.

3.2. Adsorption/desorption isotherms

Figs. 7 and 8 represent adsorption isotherms obtained for different amorphous silica samples. The characteristic shape and the maximum volume of nitrogen adsorbed obtained from the adsorption and desorption isotherms varied, depending on the type of nano- or micro-silica studied. In general, silicas produced at high temperature, such as the standard micro-silica (PmS-4 in Fig. 7) and the pyrogenic silica (PnS-3, PmS-5 and PmS-6, Fig. 8), show an isotherm shape of type IV (porous materials) according to the IUPAC nomenclature [43]. The presence of a hysteresis loop in the desorption isotherm shows that the samples are macroporous (materials with pores larger than 50 nm). The macroporosity is mainly produced by the packing effects of primary particles of a spherical shape (validated with SEM/(S)TEM analysis), and a probable contribution of mesoporosity (2–50 nm). The presence of mesoporosity is generated by the irregular shape of the silica particles in the standard micro-silica (PmS-4) and submicron silica (PnS-3) samples together with some carbon particles in the PmS-4 sample. The maximum volume of the adsorbed nitrogen is related to the pore volume of the silica samples. In general, a smaller particle size leads to a larger pore volume, as shown by sample POnS-7. This sample also has a type IV (H1) isotherm, mainly exhibited by highly agglomerated very small primary particles (11 nm).

Similarly to the other silica's studied, samples produced by the precipitation method (CnS-1 and CnS-2) show adsorption isotherms of type IV. This is characteristic for solid materials with mesoporosity, which is validated by the presence of a well-defined hysteresis loop in the desorption branch (see Fig. 7). This type of behavior is also classified by [43] as hysteresis loop H1 and H2, which are commonly found when cylindrical and bottleneck-type pores are present in the porous material. It is evident from these results that the production method determines the textural properties of the micro- and nano-silica samples.

3.3. Specific surface areas by BET (SSA_{BET}) and by t-plot method ($SSA_{t\text{-plot}}$ and SSA_{ext})

The BET specific surface areas, calculated using the parameters obtained from the isotherms and regression lines presented in Figs. 7 and 8 are summarized in Table 4 for each amorphous silica studied. Similarly to the SSA_{BET}, the total specific surface area ($SSA_{t\text{-plot}}$), the external specific surface area (SSA_{ext}) and the micropore volume (V_{MP}) were calculated using the parameters obtained from the generated *t*-plot (Figs. 9 and 10). The total ($SSA_{t\text{-plot}}$) and the external specific surface areas (SSA_{ext}) mentioned in Table 4 were computed using Eqs. (2) and (3), respectively.

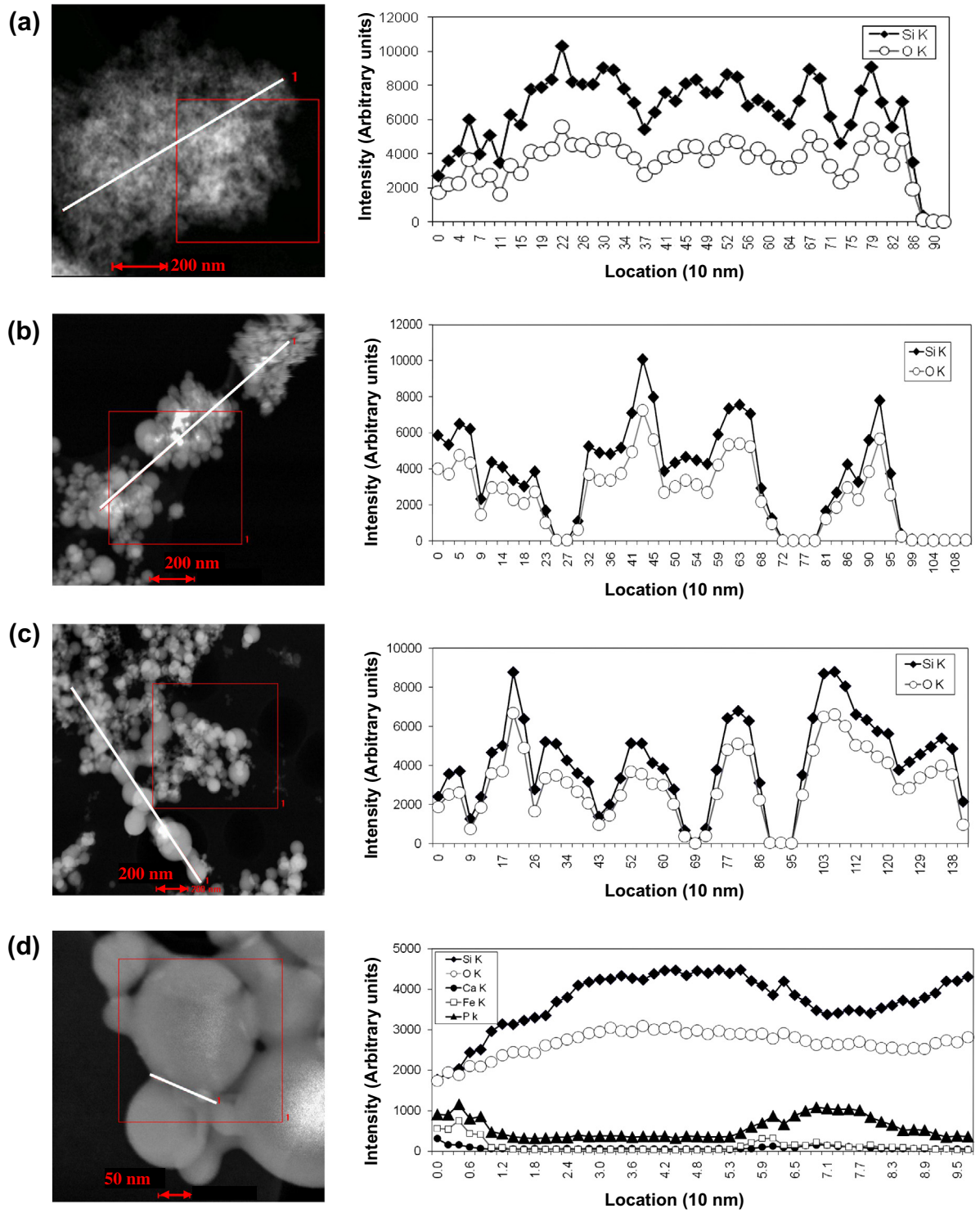

Fig. 5. High angle annular dark field (HAADF) image photomicrograph and EDS line analysis of the different silica samples studied, (a) CnS-1, (b) CnS-2, (c) PnS-3 and (d) PmS-4.

From the textural parameters computed for all the silica samples, important observations can be made. As to be expected the SSA_{BET} is larger with smaller silica particles. As the mean size of the silica particles depends on the production procedure, so does the SSA_{BET}. The size of the primary particles and the production method defines the type of the isotherm (Table 4, Figs. 7 and 8). Sample CnS-1 synthesized from waterglass precursors shows the highest SSA_{BET} of all investigated commercial nano-silicas, due to its content of micropores (51×10^{-4} cm^3/g), as is shown in Table 4. On the other hand, micro-silica (PmS-4) and synthetic silica (PmS-6) produced at high temperature show a low microporosity (5–14×10^{-4} cm^3/g) and a SSA_{BET} (less than 24 m^2/g).

The two pyrogenic silica samples (PnS-3 and PmS-5) show values of SSA_{BET} and SSA_{ext} similar to the sample CnS-2. These three samples have the same micropore volumes (around 27×10^{-4} cm^3/g). The only differences displayed by these samples are

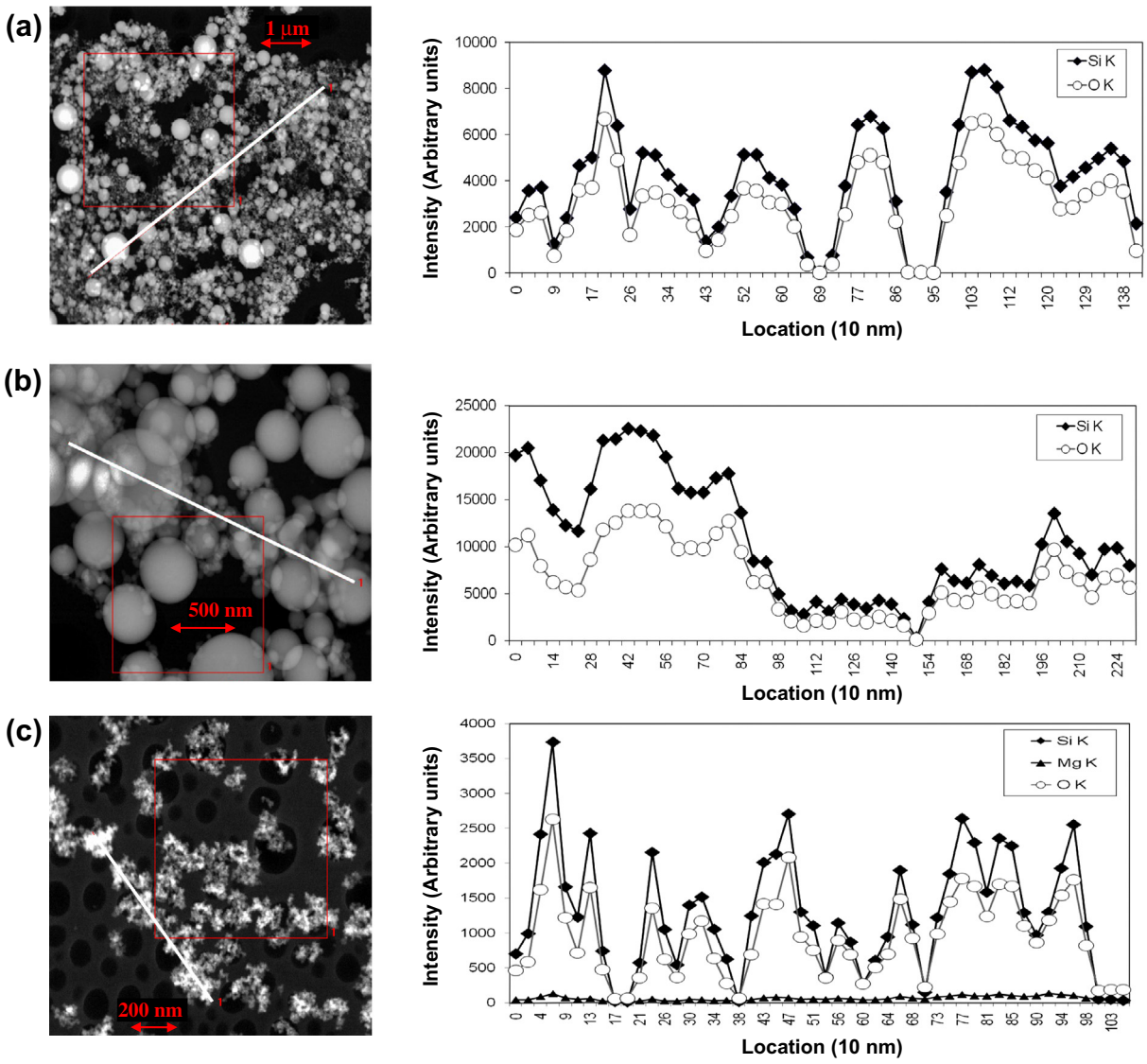

Fig. 6. High angle annular dark field (HAADF) image photomicrograph and EDS line analysis of the different silica's, (a) PmS-5, (b) PmS-6 and (c) POnS-7.

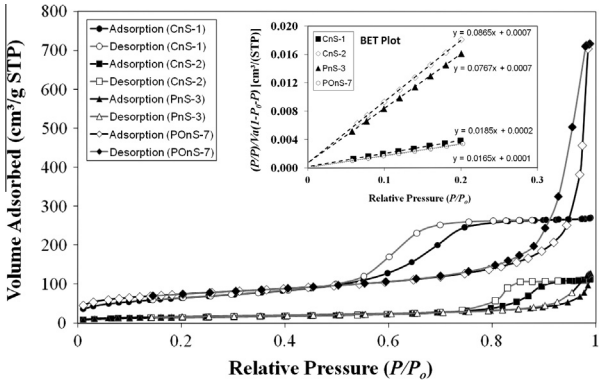

Fig. 7. Nitrogen adsorption/desorption isotherm for nano-silica samples.

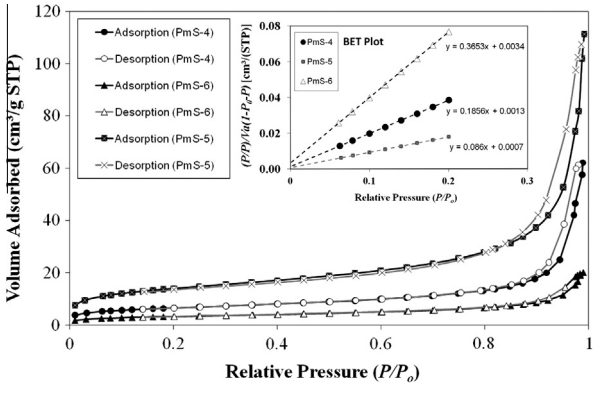

Fig. 8. Nitrogen adsorption/desorption isotherm for micro-silica samples.

in the maximum amount of gas adsorbed, and hence, in the pore volume. Also, the pore-size and pore distribution (discussed later in Section 3.4) are different. The difference between the SSA_{BET} and SSA_{ext} specific surface areas varies between 7% and 26% for the investigated samples. The variation in SSA_{BET} and SSA_{ext} can be reduced by employing other models to calculate the layer thickness and micropore volume, as was stated by [11]. For that reason, the total specific surface areas ($SSA_{t\text{-plot}}$), which includes all the pores, were determined from the slope of the straight line segment passing though the origin at the pressure regions (P/P_0) lowers than 0.10 using Eq. (3), as shown in Table 4. In these conditions a

multimolecular adsorption is taking place as was established by [44]. This surface area will not always be exactly equal to SSA_{BET} [17], which is the case of samples CnS-1 and POnS-7. The points where the slope of the straight lines changes can give indication of the pores structure of the silica samples studied. At higher relative pressures (higher t values) deviations from a straight line occur. Lippens and De Boer [17] distinguished three cases: (a) the surface is freely accessible up to high relative pressures; the multilayer can form undisturbedly on all parts of the surface; the adsorption branch of the isotherm has entirely the shape of the t-plot curve; the volume adsorbed-layer thickness plot (V_a–t) is one straight line (case of sample PmS-6); (b) at a certain pressure capillary condensation will occur in pores with bottleneck shapes and dimensions; the material takes up more adsorbate than corresponds to the volume of the multilayer; the adsorption branch lies above the t-plot curve; the slope of the V_a–t plot increases (the case of sample CnS-1); (c) in slit-shaped pores or large holes capillary condensation is not possible unless at very high relative pressures, then the free space in the pores becomes smaller owing to the growth of the adsorbed layer but at a certain moment the pore may be completely filled by the adsorbed layer on both pores parallel walls, the V_a–t plot will now get a smaller slope, corresponding to the surface area still accessible (mainly the case of sample POnS-7 and to a lower extent with samples PmS-4 and PmS-5).

The nano-silica produced from olivine represents a special case. This silica has the maximum volume of adsorbed gas (720 cm^3/g STP) and thus the largest pore volume of all samples studied. The volume of nitrogen adsorbed per gram is more than twice that exhibited by the colloidal nano-silica with the smallest particle size (CnS-1). This difference is due to the micropore volume of the sample POnS-7 (297×10^{-4} cm^3/g), which is one order of magnitude higher than the rest of silica samples studied. The high micropore volume is the result of the agglomerated state of small particles in three dimensions (3D network). Thus, POnS-7 is formed by primary particles (10–20 nm), agglomerated in clusters (secondary particles). These agglomerates are responsible for the large volume of adsorbed gas and for the presence of micro, meso and macropores (see Figs. 1g and 3c). The highly agglomerated state that probably produced slit-shaped pores explains also the large difference between the total surface areas calculated (263 and 276 m^2/g for SSA_{BET} and $SSA_{t\text{-plot}}$, respectively) and the external specific surface area (194 m^2/g for SSA_{ext}). Also, the highly agglomerated state is confirmed taking into account the arbitrary agglomeration ratio (d_{agg}/d_{BET}) calculated for sample POnS-7 (Table 4), which is the highest comparing to with the rest of the silicas studied (d_{agg}/d_{BET} between 0.1 and 4.8).

In contrast to the results of the SSA_{BET}, the values of the SSA_{ext} (Table 4) clearly show that CnS-1 has the maximum external specific surface area (217 m^2/g), while the POnS-7 has 194 m^2/g. This result is expected because the average primary particle size of the CnS-1 defined by DLS is in the range of 0.9–2.3 nm and the primary particle sizes of the olivine nano-silica is between 10 and 20 nm. Nevertheless, the calculated $SSA_{t\text{-plot}}$ is higher than the SSA_{BET} for the case of POnS-7, which suggests the presence of smaller silica particles in clusters.

Different values of the specific surface area and the presence of a high or low micropore volume in the silica samples studied would have consequences for the concrete performance. Obviously, due to the difference between the surface characteristics (total or internal surface area, micropore volume, content of silanol group, etc.), a nano-silica with a specific surface area of 50 m^2/g cannot perform as a nano-silica with a specific surface area of 300 m^2/g in concrete mixtures. Various researchers [45–47] have reported some different results attributed to the type and surface areas of nano-silica. They found that colloidal, precipitated and pyrogenic nano-silicas are in the form of relatively large aggregates (similar to the results presented previously) and, although applying different dispersion methods could affect their initial aggregation status in water, it could not break them into single particles. Furthermore, they demonstrated that the ionic composition of the fluid in the pores could significantly influence the stability of nano-silicas and could lead to their aggregation inside the concrete cementitious matrix. An important finding reported by Madani et al. [46] is the fact that the surface area of the nano-silica is significantly affecting the pozzolanic reactivity. It can, therefore, be expected that the samples CnS-1 and POnS-7 should display a higher pozzolanic activity. Nevertheless, it has been reported [45–47] that the extent of aggregation of the silica particles and the presence of microporosity are additional influencing factors. For example, due to a higher extend of aggregation of the nano-silica particles that leads to a larger pore volume, a considerable amount of water is adsorbed in the pores of the aggregates, resulting in the reduction of the water available to lubricate the granular system and for hydration of cement; consequently, a lower flowability and a lower extend of hydration result [47]. In general, at any given replacement level, the workability of cement pastes would decrease as the surface area of the nano-silica increases. In addition, it was demonstrated that the C—S—H gel precipitated in the surface of the nano-silica aggregates has less favorable mechanical properties (cannot function as a binder) and higher porosity than the gel produced by well dispersed silica nano-particles [47,48]. The presence of an interparticle transition zone (ITZ) between the large reacted agglomerates and the bulk paste has been reported, which acts as a weak zone that decreases the final mechanical properties of concrete. Based on this consideration and the fact that the sample POnS-7 presents the highest agglomeration state and microporosity, a lower flowability can be expected for this type of nano-silica.

3.4. Pore diameter and pore-size distribution (BJH method)

Fig. 11 represents the pore diameters and pore-size distribution of the selected silica samples calculated from the adsorption and desorption branches. The difference between both pore-size distributions is related to the shape of the pores. Larger differences mean more bottleneck-type of pores [29].

From the pore-size distributions of the samples studied (see Fig. 11), it is evident that the silica produced by the precipitation route from waterglass (CnS-1 and CnS-2) shows the smallest pore diameter (d_p), 5–6 nm and 11–13 nm, respectively. From the distribution of the pore sizes and the shape of the t-plot, the CnS-1 sample has bottleneck-type pores (also confirmed by the shape of the desorption isotherm) and CnS-2 has slit-shaped pores produced by the content of small particles. The pores-size distribution is also influenced by the high content of silanol groups on the surface, as was previously reported for this type of amorphous nano-silica [6]. Another finding is that the pore diameter calculated for the CnS-1 sample is larger than the sizes of the primary particle (0.9–2.3 nm). Probably this is due to the fact that the BHJ method only considers the pore-size distribution between the agglomerates. Additionally, the BHJ method employs some approximations that are not valid for very small particles or can only be applied to a given part of the isotherm as was stated by [30]. Another factor affecting the porous structure of the silica's could be the drying procedure. As explained in the experimental procedure, the silica samples were dried overnight at 105 °C for 24 h prior to the measurements. The drying procedure may affect the micropore structure of the silica CnS-1, due to coalescence of very small silica particles. Coalescence of silica particles will influence the textural characteristics, such as SSA_{BET}, pore diameter, and pore-size distribution.

Silica samples produced at high temperatures, such as PnS-3, PmS-4, PmS-5, and PmS-6, on the other hand, have average pore

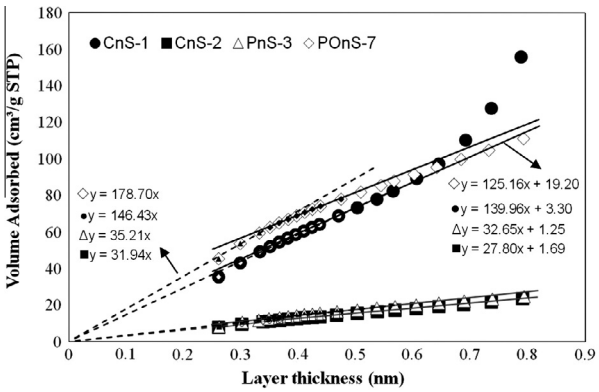

Fig. 9. *t*-Plots of the nano-silica samples; regression lines ($P/P_0 < 0.1$) for determination of the total specific surface area ($SSA_{t\text{-plot}}$); and regression lines ($0.10 < P/P_0 < 0.35$) for determination of external specific surface area (SSA_{ext}).

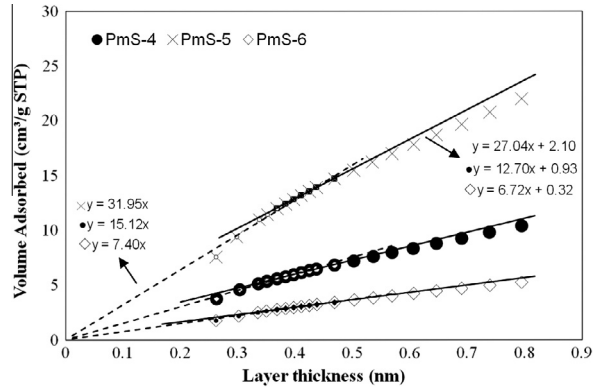

Fig. 10. *t*-Plots of the micro-silica samples; regression lines ($P/P_0 < 0.1$) for determination of the total specific surface area ($SSA_{t\text{-plot}}$); and regression lines ($0.10 < P/P_0 < 0.35$) for determination of external specific surface area (SSA_{ext}).

diameters in the range of 2–50 nm (mesopores). Nevertheless, some of them have macropores (larger than 50 nm), which is typical for packed spheres. The presence of macropores is presumably due to the predominant spherical shape of the silica particles of the PmS-4 and PmS-6. From the small difference in the average pore diameter calculated from the desorption and the adsorption branches, it can be concluded that the pores of these silica's are cylindrical (also confirmed by the shape of the *t*-plot curve for sample PmS-6).

Similar to the pyrogenic and fumed silica, sample POnS-7 has pore diameters in the mesoporous and macroporous ranges (average between 21 and 23 nm). When this silica is compared with the pyrogenic silica's, the sole distinction is the large difference in pore diameters calculated from the adsorption and the desorption branches of the isotherms. The large difference can only be due to pore-blocking effects, produced by bottleneck-type or slit-shaped pores. These pores are produced by the strongly agglomerated primary silica particles. The small agglomerated silica particles are enclosing pores with small entrances (interstitial pores). The large number of silanol groups on the silica surface can contribute to appreciable difference in pore-size distributions calculated from the adsorption and the desorption branch. Liefink reported [11] similar behavior for other nano-silica particles also prepared by the dissolution of olivine in acid. In addition, the shape of the *t*-plot curve suggests also the presence of slip-shaped pores.

3.5. Specific density by glass and helium pycnometry

The values obtained from the density measurements are shown in Table 5 and Fig. 12. Table 5 represents additionally a comparison between the results obtained by the glass and helium pycnometer.

The density values are in the expected range for the different silica samples. The specific density of the micro-silica is in the range from 2.2 to 2.3 g/cm^3, as previously reported [6]. Silica samples PmS-4 and PmS-6 showed also values in this range. Pyrogenic silica samples, with their high content of nano-particles (PnS-3 and PmS-5), showed, however, a lower specific density (ranging between 1.9 and 2.2 g/cm^3). The low density of the nano-silica is due to its content of silanol groups on the surface and the presence of micropores, as demonstrated by their pore-size distribution (see Section 3.4). The same phenomenon was also observed for the POnS-7 sample, which display low density values due to their high amount of water (surface silanol groups and a second layer of adsorbed water molecules) and their meso and macroporosity due to its strongly agglomerated state. The strong tendency to adsorb water is shown in Fig. 12, where difficulties to completely degas the sample were observed in the first cycles of density measurements.

The specific density values obtained by the helium and the glass pycnometer are similar. The helium pycnometer produces more accurate results than the glass pycnometer (difference less that 5%). Another difference between both techniques is the required time; 12 measurements in a helium pycnometer take about 30 min, and a measurement using the glass pycnometer takes about 1 day, while a room of a controlled temperature is needed.

3.6. Behavior of standard mortars with nano-silica in fresh and hardened state

Fig. 13 represents the relation between the slump-flow diameter and the total specific surface area of the mortars. It is evident that the rise in specific surface area due to the addition of nano-silica with different PSD decreases exponentially the slump-flow value of the mortars of the same SP content. The larger specific surface area lowers the free water available for lubricating the granular system. The presence of a significant number of particles enhances the number of contact points between the particles. The internal friction of the system was raised, thus reducing the slump-flow. Several researchers [49–54] have demonstrated that the slump or slump-flow is related to the viscosity and yield point of cement paste or mortar. Similarly, Bentz et al. [55] found that the plastic viscosity rises linearly with the growth of the total specific surface area of the mix. The authors additionally found that the yield stress also increases linearly with the computed particle number density. The particle number density is the power law proportionality between the particle density and the measured yield stress, normally used in percolation approaches [55]. For that reason, the observed reduction in the slump-flow value is a consequence of changes in the viscosity and yield point of the paste due to the presence of nano-particles. Nevertheless, based on the deviation (error) of the obtained experimental points (Fig. 13), it is evident that other factors also influence the measured slump-flow diameter. These factors can include: changes in the hydration kinetics due to differences in the density of silanol groups on the nano-silica surface, the presence of microporosity that takes up more water, interaction between the SP and the different impurities (C, S, Na and K) and the final void fraction (packing) of the mix. The void fraction is normally affected by the ability of the particles to be arranged in a close packing configuration. The ability is a function of the shape, size and compaction energy. In the case of nano-particles, due to the high Van der Waals forces between the particles, it is difficult to achieve the maximum packing. Evidence of this difficulty is the fact that the silica's CnS-2, PnS-3 and POnS-7 show similar slump-flows. It was expected that

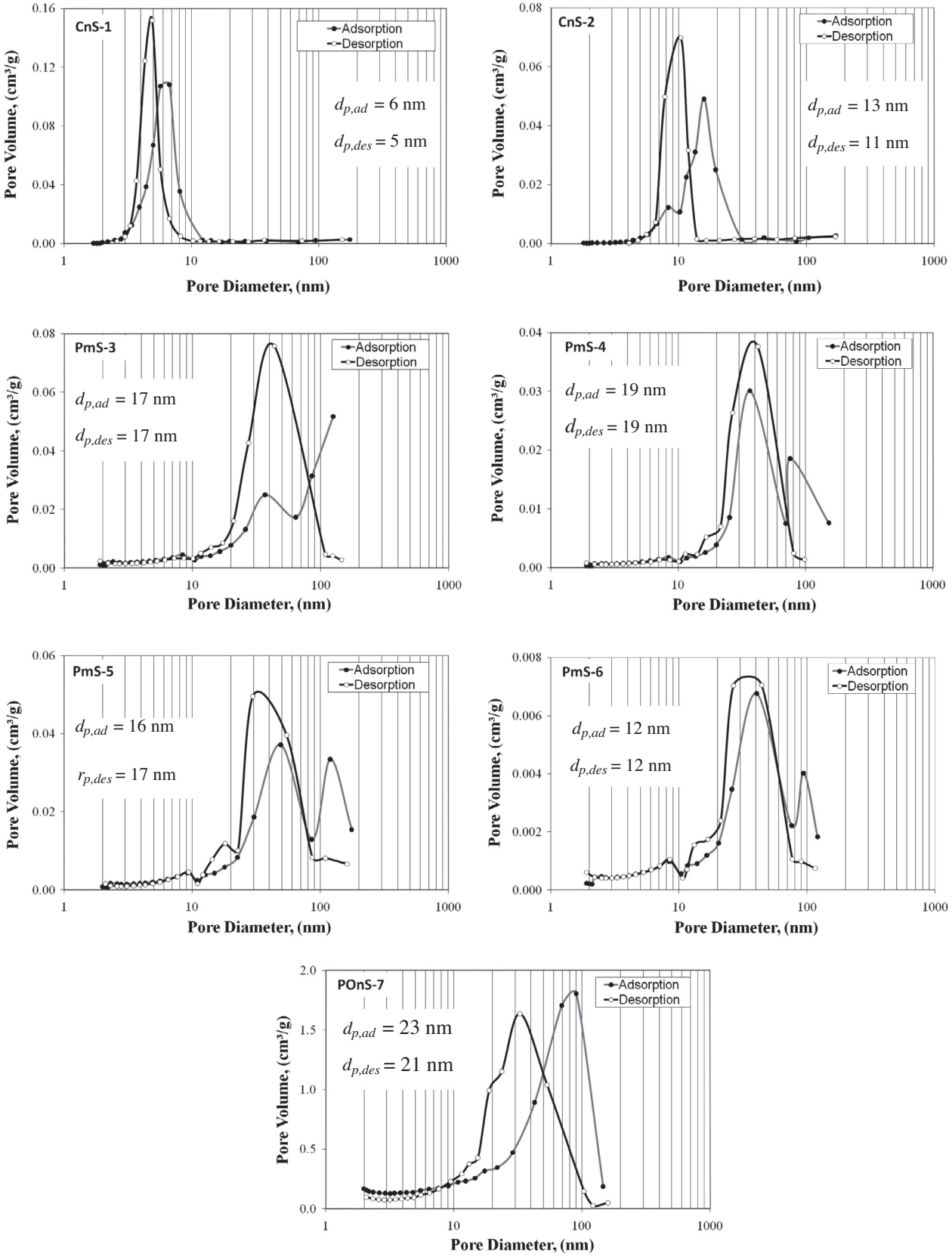

Fig. 11. Pore-size distributions of the silica's as calculated from the adsorption and desorption branches.

sample POnS-7 had a lower slump-flow diameter due to its smaller primary particle size (reflected in higher SSA_{BET}) as compared to CnS-2 and PnS-3. Apparently, the highly agglomerated state of the silica particles of POnS-7 influenced the results. One particular case was the sample CnS-1, which showed a very small slump-flow (almost zero) when a higher amount of SP (3.6% bwob) was added to

obtain a mortar capable to be mixed. CnS-1 is a colloidal nano-silica with 15% solid content produced by the waterglass route. This material has the smallest particle size (0.9–2.3 nm) of all the studied nano-silicas. Apparently, the replacement level used in this experiment (7% bwoc) was too high to produce a flowing mortar, mainly because the water in the colloidal suspension was not free water. It is partially adsorbed and retained in the surface of the nano-particles. With smaller silica nano-particles the rate of cement hydration is also enhanced [56]. Different optimum concentrations of nano-silica have been reported. For example Said et al. [57] reported that at all curing ages, the strength generally increased with the addition of nano-silica (80 m^2/g) up to 6% bwoc. Korpa et al. [58], on the other hand, reported for a pyrogenic nano-silica (200–300 m^2/g) that the optimum content is between 2% and 4% bwoc, higher contents resulted in lower workability and final strengths values. Similarly, Stefanidou and Papayianni [59] mentioned an optimum amount ranging between 1% and 2% bwoc for pyrogenic silica with a BET specific surface area of 200 m^2/g. Based on these findings and the results obtained, it is evident that the optimum amount of nano-silica in cement mortars depends on their specific surface area and would be lower than 7% for the silica with the smallest silica particles tested.

The remarkable decrease in workability produced by addition of nano-silica to cement pastes, which are observed also after the addition of a superplasticizer (SP), suggest that the high specific surface area is not the only controlling parameter in producing the significant increase in the yield stress and in the plastic viscosity. Some researchers reported [46–48] a strong and "instantaneous" interaction between silica nano-particles (no matter its state: colloidal, powder or in slurry) and some chemical species dissolved in the liquid phase of fresh cement pastes, leading to formation a destabilizing gel with high water retention capacity (in form of bound water). The results of slump-flow tests on the pastes made with the micro- and nano-silica produced by different routes support this explanation. It was, furthermore, demonstrated, similarly to the present study for samples PmS-4 and PmS-6 that the nano-particles in silica powders are often in an aggregated (firmly-held clusters) or agglomerated (loosely-held clusters) form with a final cluster size from nanometers to as high as 100 μm due to their very high specific surface area [35]. Even in a well-dispersed colloidal dispersion, the nano-particles still exist as aggregates when they are incorporated into the highly alkaline environment that exists in the cement pastes [45]. By using colloidal silica as CnS-1 and CnS-2, it is assumed that the mono-dispersed nano-particles (as was demonstrated by the DLS and LLS test results) can act as fillers and seeds much more effectively than the agglomerates of silica particles generated from powders or slurries. Nevertheless, Kong et al. [45] revealed that the colloidal silica reacts to a gel or coagulates immediately when the cement is mixed into the water containing sol due to the rapid increase of ionic strength in the paste, the rising pH, and the adsorption of Ca^{2+} ions on the silica particles. As a result, no matter what source of nano-silica is used, it is the behavior of the final agglomerates, rather than that of the individual nano-particles, which controls the flowability, the filling, the pozzolanic and acceleration effects on the cement hydration, and the improvement of the final concrete microstructure.

The strong effect of the microporosity on the slump-flow of the mix is partially validated by Fig. 14, which shows that the slump-flow decreases exponentially with an increase of the micropore volume (V_{MP}) of the nano-silica particles. The increase in the V_{MP} reduces the free water, due to the uptake of water explained above and in Section 3.3, and consequently the slump-flow drops. This trend is evident for all the silica's samples studied except for the POnS-7. The olivine nano-silica exhibited the highest difference between the total ($SSA_{t\text{-plot}}$) and external surface area (SSA_{ext}) and thus, the highest agglomeration ratio (d_{agg}/d_{BET} of 9.5). The agglomerated state can explain the results considering the high water retention capacity generated by the elevated microporosity, which is one order of magnitude higher than that of the other samples studied. Nevertheless, further research is required to establish whether additional factors are contributing to the effect on the slump-flow of the nano-silica particles produced by olivine dissolution in acid.

Figs. 15 and 16 represent the 28-day mechanical properties of the mortars. The results of the flexural strength (Fig. 15) show that the best performance was obtained with the standard micro-silica sample (PmS-4) and the lowest value was obtained with CnS-1. Similar behavior was also found for the 28-day compressive strength which is given in Fig. 16. As can be observed, the strength (compressive and flexural) was improved in general by incorporating pyrogenic type micro- and nano-silica (PnS-3, PmS-4, PmS-5 and PmS-6) and colloidal silica CnS-2. However, the strength was enhanced more significantly when incorporating PmS-4 (32% more in comparison with the blank mortar), whereas no improvement was reached by the use of CnS-1 and POnS-7 (8% lower in average). The effects on the strength can be related to the state of agglomeration within the different silica's and thus to their water retention capacity, resulting in reduction of water available for hydration of cement and consequently in lower degree of hydration of cement at age of 28 days. A higher degree of hydration of cement pastes containing micro-silica as compared to the pastes containing colloidal nano-silica has been reported [46]. The authors suggested that the lower water absorption capacity of micro-silica (pyrogenic type) causes the higher hydration. As was explained in Section 3.3, the C—S—H gel precipitated on the surface of the nano-silica aggregates, may, moreover, have lower mechanical properties (cannot function as a binder) and higher porosity than the gel produced by well dispersed silica nano-particles [47,48]. The presence of an ITZ between the large agglomerates with a modified surface after reaction and the bulk paste, which act as weak zone may decrease the final mechanical properties of the mortars. This assumption was validated by the fact that the sample POnS-7, which has the highest agglomeration ratio and microporosity, shows a lower flexural and compressive strength.

Taking into account the 28-day compressive strength of the reference mortar, it was possible to calculate the relative pozzolanic index of the different nano-silica's. The results show (Fig. 17) that the colloidal nano-silica CnS-1 has the lowest pozzolanic index (91%) as compared with the others types of nano-silica tested. In general, the waterglass silica (CnS-2) and the pyrogenic silicas (PnS-3, PmS-4, PmS-5 and PmS-6) exhibit pozzolanic indices higher than 100% (in the test condition). The results suggest that the specific surface area of the silica is a significant factor with the pozzolanic activity. The low pozzolanic index (92%) of the olivine nano-silica is probably caused by the presence of relatively large agglomerates of very small silica particles within this silica. Since only the external surface of the agglomerates can participate in the pozzolanic reaction and the material transport within the narrow pores of the conglomerates is very slow, the pozzolanic activity of the silica from olivine can be expected to be low. It is thus possible that the significant aggregation of CnS-1 and POnS-7 in the cement matrix of the mortar is one of the main reasons for the lower pozzolanic index as compared to pyrogenic micro- and nano-silica samples of a lower specific surface area. Another factor, to be considered is that at 7% replacement of cement, the maximum wet packing is probably not obtained, which results in a lower strength.

It is important to note that no clear quantitative relations between the mechanical properties and the morphological and textural properties of the silica have been obtained. Nevertheless, some observations can be made. The nano-silica samples with

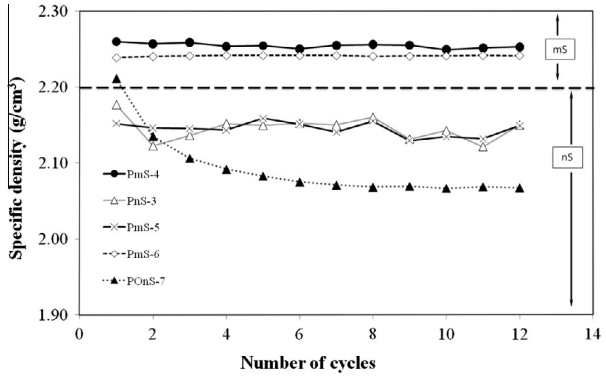

Fig. 12. Specific densities vs. the number of measured cycles.

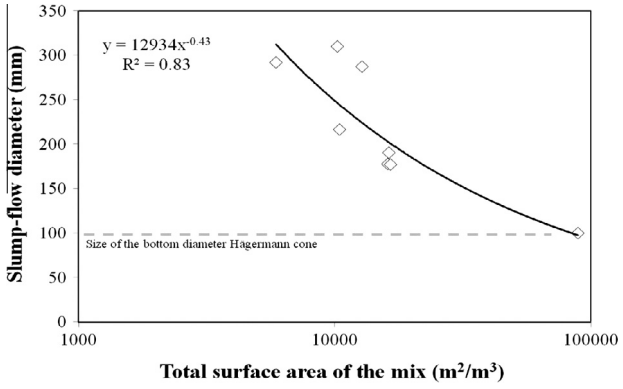

Fig. 13. Relationship between the slump-flow diameters of the mortars after 15 strokes [64] and the total surface area of the mix (cement, sand and silica).

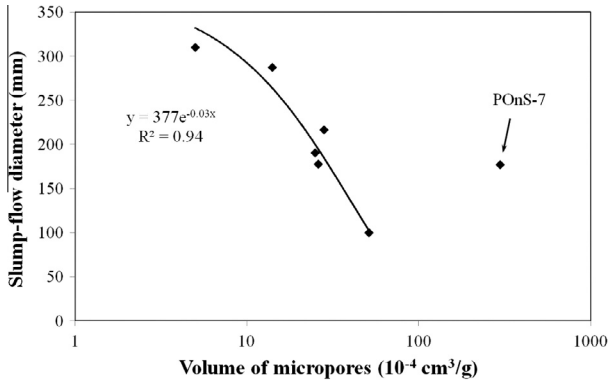

Fig. 14. Relationship between the slump-flow diameters of the mortars after 15 strokes [64] and the micropore volume (V_{MP}) of the silica's.

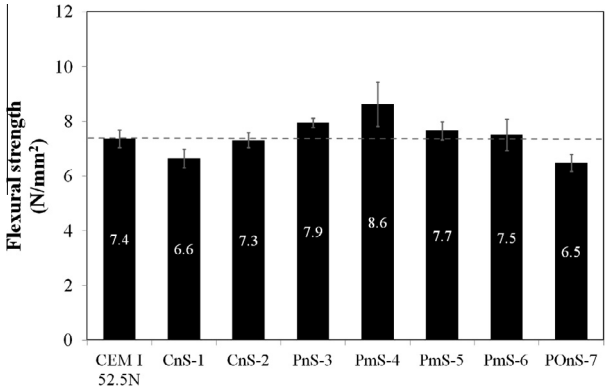

Fig. 15. 28-Day flexural strength (three point bending test) of standard mortar with silica.

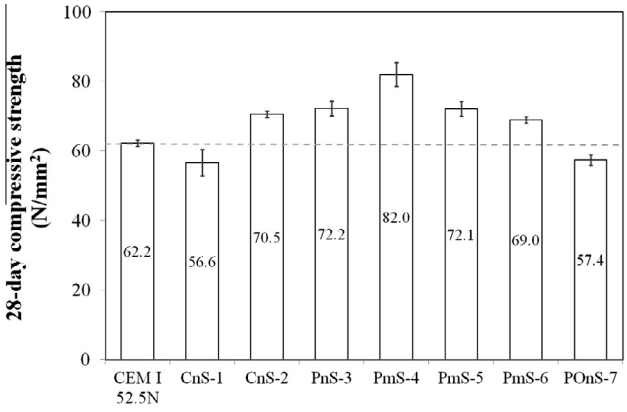

Fig. 16. 28-Day compressive strength of standard mortar with silica.

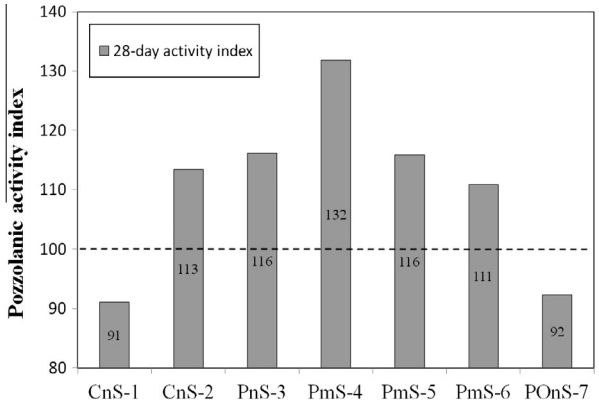

Fig. 17. 28-Day pozzolanic activity index of standard mortar with silica.

the highest specific surface area (smaller primary particle size) exhibited the lowest performance. The low performance can be attributed to their reactivity (CnS-1) and, particularly, due to particle dispersibility (agglomeration) in the cement paste (POnS-7). Dispersibility and, hence, agglomeration is an important parameter when nano-particles are added to cement paste. Sample CnS-1 was added as a well dispersed colloidal suspension and POnS-7 was added in powder form. The olivine nano-silica has particles which are agglomerated in a 3D network with a strong bond between the particles, principally due to its production route (low pH). This agglomerated state does not allow the mix to obtain the maximum packing and, possible due to the presence of larger microporosity, it can produce voids and thus raise the void content. The performance of CnS-1 can be attributed to its high reactivity. It has very small particles with sizes in the range of 0.9–2 nm and a high content of sodium (2.5% of Na_2O) as can been seen in Table 2. Land and Stephan [56] demonstrated, using isothermal calorimetric techniques, that the addition of nano-silica at the same mass concentration, but with smaller particle size (7 nm vs. 295 nm) increases the heat release by the C_3S accelerated hydration rate. The smaller particles have larger effects on the behavior of the sulfate containing phases (AFm) in the cement paste. This phenomenon can lead to a faster setting, increasing the viscosity and

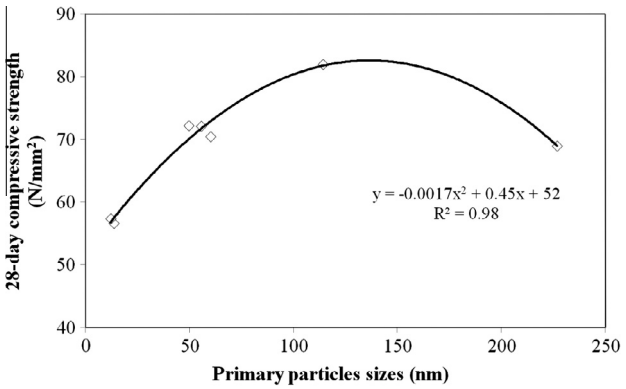

Fig. 18. Relations between 28-day compressive strength and the diameter of the primary silica particles (d_{BET}) computed by the SSA_{BET}.

Table 5
Computed densities of the silica's (helium and glass pycnometry).

Name	Helium pycnometry (g/cm^3)	Glass pycnometry (g/cm^3)	Difference (%)
CnS-1	N/D	1.10$^{(*)}$	–
CnS-2	N/D	1.39$^{(*)}$	–
PnS-3	2.146 ± 0.012	2.101	2.1
PmS-4	2.253 ± 0.023	1.39$^{(*)}$	–
PmS-5	2.145 ± 0.009	2.049	4.5
PmS-6	2.241 ± 0.001	2.187	2.4
POnS-7	2.070 ± 0.003	N/D	–

(∗): Measured in colloidal or slurry form at 22 °C.

producing a self-desiccation of the mortar. The increase in the setting rate was partially demonstrated by the necessity to use large amounts of SP (3.6% bwob) to obtain a mixable mortar. Another interesting finding is the fact that the nano-silica additives of the same SSA_{BET} result in similar compressive strengths. This is displayed by the silica's CnS-2, PnS-3 and PmS-5, the pozzolanic index of which varied between 113 and 116. Apparently, as was demonstrated in the slump-flow test results, the specific surface area is the controlling factor. Comparing, on the other hand, the results of the samples PmS-4 and PmS-6, which have SSA_{BET} of 23 and 10 m^2/g, respectively, a clear influence of the aggregation ratio is evident. Other factors, such as the presence of impurities, the shape of the silica particles, and the PSD may affect the results. The fact that the PmS-4 silica performed the best is related to its lower reactivity at early age and its wider PSD that produced a better packing (reduced void fraction) under the test conditions. Korpa et al. [58] demonstrated the low reactivity of micro-silica. The investigation of Korpa et al. [58], comprising pH-measurements and X-ray transmission microscope images (TXM), confirmed the low pozzolanic reactivity for micro-silica products, which was much lower than that achieved for fumed nano-silica dispersions. Further research is needed to understand the strength development of mortar with different nano-silicas and the influence of the application method (powder, colloidal dispersion or slurry form). Furthermore, the optimum replacement ratio for each type of nano-silica needs to be determined.

Even though no direct quantitative relation was found with the morphological characteristics obtained in this investigation, a thorough analysis taking into consideration the measured SSA_{BET} to calculated the average diameter (d_{BET}) of the primary silica particles, using Eq. (4), was performed.

All the diameters, d_{BET}, thus calculated (in nm) were plotted against the 28-day compressive strength values (Fig. 18). This figure demonstrates that, based on the correlation value of the fit curve (R^2 = 0.98), the compressive strength is a function of the average diameter of the primary particles of the silica samples and thus indirectly a function of the SSA_{BET}. Apparently, an optimum value of d_{BET} (around 135 nm) is needed to obtain the maximum compressive strength at the same w/c ratio and mass concentration of nano-particles provided the nano-silica particles are well dispersed. To the authors' knowledge, it is the first time that this is reported. The presence of a maximum or optimum value can be related (in addition to the particles reactivity and aggregate behavior) with the point where the best packing is obtained. The theories of "filling gap materials" can be used to partially explain the results [60–62]. Some researchers found for mixes of granular materials with a large difference in their average particle size, that it is possible to achieve maximum packing and, consequently, a minimum void fraction and increased compressive strength. This effect becomes predominant for a difference larger than 10 in the size ratio, and preferably between ten and one hundred [63]. The average particle size of cement used is around 13 μm and the optimum value found in Fig. 18 is around 135 nm (100 times less than cement). Apparently, this size ratio contributes to obtain the maximum compressive strength. Nevertheless, still more research is needed to validate this hypothesis and also more tests with representative samples with average primary particles sizes in the range of 120–200 nm are required.

In summary, even though the studied amorphous nano-silicas have different textural properties such as pore diameter, pore-size distribution, pore volume, and shape, apparently, the main parameters that affect the slump-flow diameter and the final mechanical properties are their specific surface area (SSA_{sph}), the average primary particle sizes, the micropore volume and size of aggregates of the silica particles. There was not any direct evident influence on the mortar properties related with the silica's pore diameter and pore-sizes distribution.

4. Conclusions

In the present work, the morphological and textural characteristics of amorphous micro- and nano-silica additives manufactured by different routes, such as precipitation from waterglass and olivine dissolution in acids, flame hydrolysis and condensation of silica fume, were studied thoroughly. The effects in the slump-flow test

Table 6
Mix design of standard mortars.

Materials (g)	Reference	CnS-1	CnS-2	PnS-3	PmS-4	PmS-5	PmS-6	POnS-7
CEM I 52.5N	450.0	418.5	418.5	418.5	418.5	418.5	418.5	418.5
Micro-/nano-silica$^{(+)}$	0	210.0	63.0	31.5	63.0	31.5	31.5	31.5
Water	225	46.5	193.5	225	193.5	225	225	225
Standard sand	1350.0	1350.0	1350.0	1350.0	1350.0	1350.0	1350.0	1350.0
SP (Glenium® 51)	2.70	16.2$^{(*)}$	2.70	2.70	2.70	2.70	2.70	2.70
SP (% bwob)	0.60	3.60	0.60	0.60	0.60	0.60	0.60	0.60
w/c	0.50	0.50	0.50	0.50	0.50	0.50	0.50	0.50
Slump-flow (mm)	292 ± 1	100 ± 0	178 ± 1	191 ± 6	288 ± 1	217 ± 2	310 ± 1	178 ± 4

(+): Powder, colloidal or slurry form; (∗) minimum needed to have a mixable mortar.

and the mechanical properties of mortars formulated with the silica samples were discussed. In addition, the implications of the silica characteristic towards the fresh and hardened properties of concrete were established. Based on these considerations, several conclusions can be drawn:

- The most observed morphology of the silica particles in the samples is spherical; changing to more irregular (angular) when the size of the particles is reduced. The presence of angular particles depends on the producing route of the silica's. In the case of the silica precipitated by waterglass and by the dissolution of olivine in acids, the angular particles are the results of agglomeration of very small particles. For the pyrogenic silicas, in addition to the impurities and clustering of small particles, the presence of angular particles is the result of the sintering of spherical particles.
- The powder nano-particles (pyrogenic and fumed silica) are often in an aggregated (firmly-held clusters) or agglomerated (loosely-held clusters) state with a final aggregate size from a few nanometers to as high as 13 μm, whereas colloidal silica samples are often present in mono-dispersed form. The silica nano-particles coming from the dissolution of olivine in acids are present in a polydisperse form with very small particle in a highly agglomerated state.
- The silica samples are amorphous and are mainly composed of SiO_2 with small amounts of impurities (Ca, P, C, Mg and Fe). The type and amount of impurities depend on the production route of nano-silica (condensation, pyrolysis or precipitation).
- The maximum volume of physically adsorbed nitrogen and the shape of the adsorption/desorption isotherm depend on the production routes of the nano-silica particles. The nano-silica obtained from the olivine mineral dissolution had the larger BET and *t*-plot specific surface area. The silica obtained from the precipitation route using waterglass precursors has a higher specific surface area than the pyrogenic silica.
- The pore diameter and pore-size distribution depend on the production route of the silica. Precipitated silica particles have a narrow or monomodal pore-size distribution (average 6–13 nm) with a micro- and meso-porous structure. The pyrogenic silica's have larger pores (average 12–19 nm) and a predominant macro- to meso-porous structure, typically found in structures of packed spheres. The silica particles produced from olivine had the distribution of the largest pores (average 20–23 nm) with a meso-porous structure caused by the highly agglomerated state and loose packing.
- The specific density of the amorphous silica particles depends on the particle size of the primary particles, the internal pore structure, and the amount of surface and internal silanol groups. For all others factors being equal, the smaller the primary particle size, the smaller the specific density of silicas.
- A potential relationship between the total surface area of the mix (cement, sand and silica) and the slump-flow of mortar with different types of amorphous silica nano-particles was established. The higher the total surface area of the mortar, the smaller the mortar slump-flow. It was also found that the final slump-flow can be affected by the state of aggregation of the primary silica particles that leads to the presence of microporosity (with a high water retention capacity) in the nano-silica samples. The slump-flow has an exponential relationship with the micropore volume of the particles.
- Even though the amorphous silica's studied have different textural properties, such as pore diameter, pore-sizes distributions and shape, the main parameters that influence the slump-flow diameter (workability) and final mechanical properties are the specific surface areas, the micropore volumes (which defined the water adsorption capacity) and the state of agglomeration. These parameters control the filling capacity, the pozzolanic activity and the rate of hydration of the cement. It is thus suggested that the silica should be dispersed as well as possible to obtain the intended improvement of the concrete properties.

Acknowledgments

This research was carried out under the Project Number M81.1.09338 in the framework of the Research Program of the Materials innovation institute (www.m2i.nl) and The European Community's Seventh Framework Program, ProMine: Nano-particle products from new mineral resources in Europe, FP7-NMP-2008-LARGE-2 under Grant agreement 228559. The authors also wish to express their gratitude to P.R. Spiesz for his collaboration and to the following sponsors of the Building Materials research group at TU Eindhoven: Rijkswaterstaat Centre for Infrastructure, Graniet-Import Benelux, Kijlstra Betonmortel, Struyk Verwo, Attero, ENCI, Provincie Overijssel, Rijkswaterstaat Directie Zeeland, A&G Maasvlakte, BTE, Alvon Bouwsystemen, V.d. Bosch Beton, Selor, Twee "R" Recycling, GMB, Schenk Concrete Consultancy, Intron, Geochem Research, Icopal, BN International, APP All Remove, Consensor, Eltomation, Knauf Gips, Hess ACC Systems, Kronos and Joma International (chronological order of joining).

References

[1] Reinhardt HW. Beton als constructiemateriaal. Delftse Universitaire Pers., Delft, The Netherlands; 1998 [in Dutch].
[2] Sobolev K, Flores I, Hermosillo R. Nanomaterials and nanotechnology for high-performance cement composites. In: Proceedings of ACI session on nanotechnology of concrete: recent developments and future perspectives, November 7, Denver, USA; 2006.
[3] Zhu W, Bartos PJM, Porro A. Application of nanotechnology in construction summary of a state-of-the-art report. Mater Struct/Mat6riaux et Constr 2004;37(November):649–58.
[4] Gaitero JJ, Campillo I, Guerrero A. Reduction of the calcium leaching rate of cement paste by addition of silica nanoparticles. Cem Concr Res 2008;38:1112–8.
[5] Sobolev K, Ferrara M. How nanotechnology can change the concrete word – Part 1. Am Ceram Bull 2005;84(10):15–7.
[6] ECETOC JACC REPORT No. 51. Synthetic amorphous silica (CAS No. 7631-86-9). Brussels: European Centre for Ecotoxicology and Toxicology of Chemicals; September 2006. p. 1–231.
[7] Jonckbloedt RCL. The dissolution of olivine in acid, a cost effective process for the elimination of waste acids. Ph.D. thesis. Utrecht University, The Netherlands; 1997. p. 114.
[8] Dunster A. Silica fume in concrete. Information paper N° IP 5/09. Garston, UK: IHS BRE Press; 2009.
[9] Iler RK. The colloid chemistry of silica and silicate. New York: Edit. Ithaca; 1979. p. 1–250.
[10] Schuiling RD. A method for neutralizing waste sulphuric acid by adding a silicate. Utrecht University, European patent application no 8590343.5; 1986.
[11] Lieftink DJ. The preparation and characterization of silica from acid treatment of olivine. Ph.D. thesis. Utrecht University, The Netherlands; 1997. p. 175
[12] Lazaro A, Brouwers HJH, Quercia G, Geus JW. The properties of amorphous nano-silica synthesized by the dissolution of olivine. Chem Eng J 2012;211–212:112–21.
[13] Bhambhani MR, Cutting PA, Sing KSW, Turk DH. Analysis of nitrogen adsorption isotherms on porous and nonporous silicas by the BET and as methods. J Colloid Interface Sci 1971;88(1):109–17.
[14] Szekeres M, Toth J, Dekany I. Specific surface area of Stoeber silica determined by various experimental methods. Langmuir 2002;18:2678–85.
[15] Dutta D, Chatterjee S, Pillai KT, Pujari PK, Ganguly BN. Pore structure of silica gel: a comparative study through BET and PALS. Chem Phys 2005;312:319–24.
[16] Brunauer S, Emmett PH, Teller E. Adsorption of gases in multimolecular layers. J Am Chem Soc 1938;60:309–19.
[17] Lippens BC, De Boer JH. Studies on pore systems in catalysts V. The *t* method. J Catal 1965;4:319–23.
[18] Barret EP, Joyner LG, Halenda PP. The determination of pore volume and area distributions in porous substances. I. Computations from nitrogen isotherms. J Am Chem Soc 1951;73:373–80.

[19] CEN EN 13263–1+A1. Silica fume for concrete – Part 1: definitions, requirements and conformity criteria. European Commission for Standardization (CEN); 2009. p. 1–29.
[20] Cyr M, Tagnit-Hamou A. Particle size distribution of fine powders by LASER diffraction spectroscopy. Case of cementitious materials. Mater Struct 2001;34:342–50.
[21] ISO 13320-1. Particle size analysis – laser diffraction methods – Part 1: General principles. International Organization for Standardization. CH-1211 Genève 20, Switzerland; 1999. p. 1–42.
[22] Hunger M. An integral design concept for ecological self-compacting concrete. Ph.D. thesis. Eindhoven University of Technology, The Netherlands; 2010. p. 1–240.
[23] ISO 13321. Particle size analysis – photon correlation spectroscopy. International Organization for Standardization. CH-1211 Genève 20, Switzerland; 2006. p. 1–108.
[24] McCabe W, Smith J. Unit operations of chemical engineering. New York, United States: McGraw-Hill Book Company, Inc.; 1956.
[25] DIN ISO 9277. Determination of the specific surface area of solids by gas adsorption using the BET method. German Institute of Normalization (DIN); 1995. p. 1–19.
[26] De Boer JH, Lippens BC. Studies in pore system in catalysts II. The shape of pores in aluminum oxides systems. J Catal 1964;3:38–43.
[27] Harkins WD, Jura G. Surfaces of solids. XIII. A vapor adsorption method for the determination of the area of a solid without the assumption of a molecular area, and the areas occupied by nitrogen and other molecules on the surface of a solid. J Am Chem Soc 1944;66(8):1366–73.
[28] Thiele G, Poston M, Brown R. A case study in sizing nanoparticles. Micromeritics Analytical Services; 2007. p. 1. <www.micromeritics.com>.
[29] Gregg SJ, Sing KSW. Adsorption, surface area and porosity. London: Academic Press; 1982. p. 303.
[30] Groen JC, Peffer LAA, Perez-Ramirez J. Pore size determination in modified micro- and mesoporous materials. pitfalls and mimitations in gas adsorption data analysis. Micropor Mesopor Mater 2003;60:1–17.
[31] Sing KWS. Characterization of porous materials: past, present and future. Colloids Surf A Physicochem Eng Aspects 2004;241:3–7.
[32] DIN EN 1097-7. Test for mechanical and physical properties of aggregates – Part 7: determination of particle density of filler-pycnometer method. German Institute of Normalization (DIN); 1999. p. 6.
[33] CEN EN 196-1. Methods of testing cement Part 1: determination of strength. European Commission for Standardization (CEN); 2005. p. 1–36.
[34] Justnes H, Ostnor T. Pozzolanic, amorphous silica produced from the mineral olivine. In: Malhotra VM, editor. Proceedings of the 7th CANMET/ACI international conference on fly ash, silica fume, slag, and natural pozzolans in concrete, vol. II, July 22–27, Chennai, India; 2001. p. 769–81.
[35] Diamond S, Sahu S. Densified silica fume: particle sizes and dispersion in concrete. Mater Struct 2006;39:849–59.
[36] Lazaro A, Brouwers HJH. Nano-silica production by a sustainable process; application in building materials. In: Gregor Fisher, Mette Geiker, Ole Hededal, Lisbeth Ottosen, Henrik Stang, editors. 8th Fib international Ph.D. symposium in civil engineering, Lyngby, June 20–23, Denmark; 2010. p. 487–92.
[37] Lazaro A, Geus JW, Brouwers HJH. Influence of the production process conditions on the specific surface area of olivine nano-silicas. In: Proceedings of the international conference nanomaterials: applications and properties. Sumy State University, Simferopol, Ukraine, vol. 1, no 1; 2012. p. 01001(1)–(4).
[38] Lazaro A, Quercia G, Brouwers HJH. Production and application of a new type of nano-silica in concrete. In: Ibausil FA, editor. Proceedings of the international conference on building materials. Finger-Institut fur Baustoffkunde, Weimar, Germany; 2012. p 1–6.
[39] Gorrepati EA, Wongthahan P, Raha S, Fogler HS. Silica precipitation in acidic solutions: mechanism, pH effect, and salt effect. Langmuir 2010;26:10467–74.
[40] Friede B. Microsilica-characterization of an unique additive. In: Proceedings of the 10th international inorganic-bonded fiber composites conference (IIBCC 2006) – October 15–18, Sao Paulo, Brazil. Universidade de Sao Paulo and University of Idaho; 2006. p. 135–44.
[41] Plank J, Schroefl Ch, Gruber M, Lesti M, Sieber R. Effectiveness of polycarboxylate superplasticizers in ultra high strength concrete: the importance of PCE compatibility with silica fume. J Adv Concr Technol 2009;7(1):5–12.
[42] Marchuk V. Dispersibility of the silica fume slurry in cement paste and mortar. Betontechnische Berichte concrete technology reports 2001–2003. Düsseldorf, Germany: Verlag Bau + Technik; March 2004. p. 125–32.
[43] International Union of Pure and Applied Chemistry IUPAC. Reporting data for gas/solid systems with special reference to the determination of surface area and porosity. Pure Appl Chem 1985; 57(4): 603–19.
[44] De Boer JH, Lippens BC, Linsen BG, Broekhoff, van den Heuvel A, Osinga J. The *t*-curve of multimolecular N_2-adsortion. J Colloid Interface Sci 1966;21:405–14.
[45] Kong D, Du X, Wei S, Zhang H, Yang Y, Shah SP. Influence of nano-silica agglomeration on microstructure and properties of the hardened cement-based materials. Constr Build Mater 2012;37:707–15.
[46] Madani H, Bagheri A, Parhizkar T. The pozzolanic reactivity of monodispersed nanosilica hydrosols and their influence on the hydration characteristics of Portland cement. Cem Concr Res 2012;42:1563–70.
[47] Kong D, Su Y, Du X, Yang Y, Wei S, Shah SP. Influence of nano-silica agglomeration on fresh properties of cement pastes. Constr Build Mater 2013;37:557–62.
[48] Berra M, Carassiti F, Mangialardi T, Paolini AE, Sebastiani M. Effects of nanosilica addition on workability and compressive strength of Portland cement pastes. Constr Build Mater 2012;35:666–75.
[49] Roussel N, Stefani C, Leroy R. From mini-cone test to Abrams cone test: measurements of cement-based materials yield stress using slump test. Cem Concr Res 2005;35(5):817–22.
[50] Roussel N, Coussot P. Fifty-cent rheometer for yield stress measurements: from slump to spreading flow. J Rheol 2005;49(3):705–18.
[51] Saak AW, Jennings HM, Shah SP. A generalized approach for the determination of yield stress by slump and slump flow. Cem Concr Res 2004;34(3):363–71.
[52] Pashias N, Boger DV, Summers J, Glenister DJ. A fifty cent rheometer for yield stress measurement. J Rheol 1996;40(6):1179–89.
[53] Wallevik JE. Relationship between the Bingham parameters and slump. Cem Concr Res 2006;36:1214–21.
[54] Petit JY, Wirquin E, Vanhove Y, Khayat K. Yield stress and viscosity equations for mortars and self-consolidating concrete. Cem Concr Res 2007;37(5):655–70.
[55] Bentz DP, Ferraris ChF, Galler MA, Hansen AS, Guynn JA. Influence of particle size distributions on yield stress and viscosity of cement–fly ash pastes. Cem Concr Res 2011;42:404–9.
[56] Land G, Stephan D. The influence of nano-silica on the hydration of ordinary Portland cement. J Mater Sci 2012;47:1011–7.
[57] Said AM, Zeidan MS, Bassuoni MT, Tian Y. Properties of concrete incorporating nano-silica. Constr Build Mater 2012;36:838–44.
[58] Korpa A, Trettin R, Böttger KG, Thieme J, Schmidt C. Pozzolanic reactivity of nanoscale pyrogene oxides and their strength contribution in cement-based systems. Adv Cem Res 2008;20(1):35–46.
[59] Stefanidou M, Papayianni I. Influence of nano-SiO_2 on the Portland cement pastes. Composites: Part B 2012;43:2706–10.
[60] De Larrard F. Ultrafine particles for the making of very high strength concrete. Cem Concr Res 1989;19:161–72.
[61] De Larrard F, Sedran T. Optimization of ultra-high-performance concrete by the use of a packing model. Concr Res 1994;24(6):997–1009.
[62] Palm S, Wolter A. Determining and optimizing the void filling of dry particle systems. Cem Int 2009;7:2–8.
[63] Roddy G, Chatterji J, Cromwell R. Well treatment composition and methods utilizing nano-particles. Halliburton Energy Services. United States of America patent application no 20080277116 A1, November 13; 2008. p. 1–12.
[64] CEN EN 1015-3. Methods of test for mortar for masonry. Determination of consistence of fresh mortar (by flow table). European Commission for Standardization (CEN); 1999. p. 1–10.